

# IVP-VAE: Modeling EHR Time Series with Initial Value Problem Solvers

Jingge Xiao<sup>a;\*</sup>, Leonie Basso<sup>a</sup>, Wolfgang Nejdl<sup>a</sup>, Niloy Ganguly<sup>b</sup> and Sandipan Sikdar<sup>a</sup>

<sup>a</sup>L3S Research Center, Leibniz University Hannover

<sup>b</sup>Indian Institute of Technology Kharagpur

**Abstract.** Continuous-time models such as Neural ODEs and Neural Flows have shown promising results in analyzing irregularly sampled time series frequently encountered in electronic health records. Based on these models, time series are typically processed with a hybrid of an initial value problem (IVP) solver and a recurrent neural network within the variational autoencoder architecture. Sequentially solving IVPs makes such models computationally less efficient. In this paper, we propose to model time series purely with continuous processes whose state evolution can be approximated directly by IVPs. This eliminates the need for recurrent computation and enables multiple states to evolve in parallel. We further fuse the encoder and decoder with one IVP solver based on its invertibility, which leads to fewer parameters and faster convergence. Experiments on three real-world datasets show that the proposed approach achieves comparable extrapolation and classification performance while gaining more than one order of magnitude speedup over other continuous-time counterparts.

## 1 Introduction

Electronic Health Record (EHR) data contains multi-variate time series of patient information, such as vital signs and laboratory results, which can be utilized to perform diagnosis or recommend treatment [22]. The data in EHR time series is often irregularly sampled (i.e., unequal time intervals between successive measurements) and can have missing values [37]. The irregularity is caused mainly due to unstructured manual processes, event-driven recordings, device failure, and also different sampling frequencies across multiple variables [36]. These complexities make learning and modeling clinical time series data particularly challenging for classical machine learning models [30, 33]. In recent years, significant progress has been made towards developing models to handle irregularly sampled time series data [5, 27, 31, 37] and are extensively tested on EHR data.

Neural ODEs [6] are continuous-time models based on ordinary differential equations (ODEs) that can naturally handle irregularly sampled data. The data is assumed to be generated by a continuous process that is modeled using ODEs. Rubanova et al. [27] further extend the idea and develop Latent-ODE by integrating Neural ODEs and RNN into a variational autoencoder (VAE) [18] architecture. Given Neural ODE models require deploying a numerical ODE solver which is computationally expensive. Biloš et al. [3] propose an efficient alternative by directly modeling the solution of ODEs with a neural network, thereby obtaining a variant of Latent-ODE using Neu-

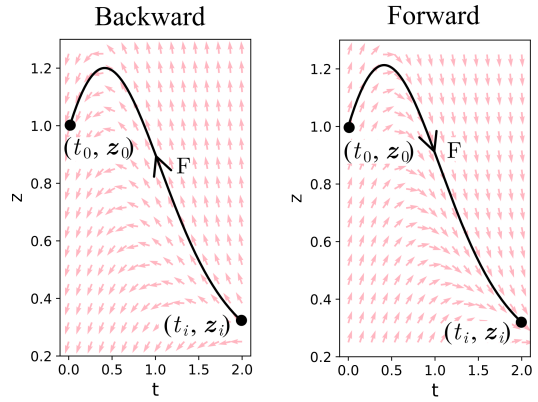


**Figure 1:** Given an example ODE  $\frac{dz}{dt} = 1 - 2 \cdot t \cdot z$ , (Left) if we take  $(z_i, t_i)$  as the initial condition, where  $z = 0.31953683$  and  $t = 2.0$ , and calculate the state at  $t = 0.0$  using an IVP solver  $F$ , we can obtain  $z = 1.0$ . On the opposite, (Right) if taking  $(z = 1.0, t = 0.0)$  as the initial condition and evolve forward in time along the slope field using  $F$ , we can obtain  $z = 0.31953683$ .  $(z_i, t_i)$  and  $(z_0, t_0)$  are on the same integral curve, one can calculate forward and backward using the same IVP solver.

ral Flows, referred to as Latent-Flow in this paper. However, when analyzing time series, these Latent-based continuous-time models (Latent-ODE and Latent-Flow) require sequential processing of data, which makes them inefficient and hard to train.

In this work, we propose IVP-VAE, a continuous-time model specifically designed for EHR time series, which is capable of dealing with irregularly sampled time series data in a non-sequential way. Different from Latent-ODE and Latent-Flow, our model takes variational approximation purely as solving initial value problems (IVPs). Specifically, observations at different time points are mapped to states of an unknown continuous process and propagated to a latent variable  $z_0$  by solving different IVPs in parallel, thereby achieving a significant speedup over existing continuous-time models. Latent-based continuous-time models use the VAE architecture, whose encoder and decoder consist of separate recognition and generative modules. We observe that IVP solvers are inherently invertible (i.e., IVPs can be solved in both forward and backward time directions, as illustrated in Figure 1) and exploit this property to fuse encoding and decoding modules by the same solver. This results in reduced model complexity in terms of number of parameters and convergence rate.

\* Corresponding Author. Email: xiao@l3s.de

We deploy our model on the tasks of time series forecasting and classification across three real-world EHR datasets. IVP-VAE generally outperforms the existing latent-based continuous-time models across all the datasets and tasks. More importantly, it achieves more than one order of magnitude speedup over its latent-based predecessors. With regard to the state-of-the-art irregular sampled time series classification and forecasting models, IVP-VAE achieves comparable results. Additionally, our model is able to achieve significant improvements in settings where the training data is limited, which is often encountered in healthcare applications (e.g., cohort of patients with a particular condition).

We summarize the main contributions of the current work below -

- We propose a novel continuous-time model IVP-VAE which can capture sequential patterns of EHR time series by purely solving multiple IVPs in parallel.
- By utilizing the invertibility property of IVP solvers, we achieve parameter sharing between encoder and decoder of the VAE architecture, and thus provide a more efficient generative modeling technique.
- Across real-world datasets on both forecast and classification tasks, IVP-VAE achieves comparable results while significantly increasing efficiency.
- IVP-VAE achieves significant improvements over baseline models in settings where the training data is limited.

## 2 Background and Related Work

EHR data contains comprehensive information about patients' health conditions and empowered the research of personalized medicine [1]. The publishing of several large EHR datasets, including MIMIC-III [16], MIMIC-IV [15], eICU [23], etc. facilitated the development of deep learning models for this domain. Specific tasks like time series forecasting and mortality prediction were widely used to test models' capability on data modeling and representation learning [12, 22, 25, 28]. Functions built upon these can be used to support early warning of deterioration, identifying patients at risk, disease recognition, etc. [10, 34]. However, EHR time series are usually irregularly sampled [37]. The time interval between consecutive observations is not fixed, and only some observations or no observations are available at each timestamp. The tensor constructed in this way has no fixed length and is very sparse [30, 36].

There has been significant progress in developing models that are naturally able to handle irregularly sampled time series as the input [30]. Several works proposed recurrent models that add decay mechanisms to learn imputed values while training [4, 17, 19]. For example, GRU-D [5] uses a temporal decay mechanism that is based on gated recurrent units (GRUs) and incorporates missing patterns. However, along with recurrent units comes the unstable gradient issue, and difficulties in long sequence modeling and parallelizing [21]. Other works introduce attention mechanisms into models for irregular time series [7, 13, 31, 35]. Raindrop [37] combine attention with graph neural networks. Drawbacks of attention based models would become severe when the input time series has long sequences, as they obtain quadratic time complexity and high memory usage [38]. Recent convolutional models for irregular time series formulate the convolutional kernels as continuous functions [9, 20, 26]. Thus, they are able to handle data with arbitrary size and irregular sample intervals, unlike standard convolutional neural networks (CNNs). However, when dealing with arbitrary length sequences, they usually need to first pad missing entries with specific values (such as zero) [26], which can introduce irrelevant data and conceal important information.

Another model family is based on ODEs to model continuous processes. Neural ODEs [6] are continuous-time models that can naturally handle irregularly sampled data. The Latent ODE model [27] uses an ODE-RNN encoder in a VAE [18] architecture. GRU-ODE-Bayes [8] combines ODE and GRU into a continuous-time version of the GRU. The solving of an ODE with a numerical ODE-Solver is computationally expensive. Neural Flow [3] proposes an efficient alternative. The solution of an ODE is modelled directly with a neural network instead of using a numerical solver. For a more detailed definition of ODE-based continuous-time models, see section 3.2. A shortcoming of current research in this area is that existing methods often require sequentially solving a large amount of ODEs, which makes the training and inference less efficient.

Our method builds on VAE-based continuous models with Neural ODE and Neural Flow as IVP solvers. We introduce a set of novel architectural designs to further improve the efficiency. An embedding layer maps the input into a latent space where the IVP solvers are deployed. We eliminate the need for recurrent and sequential computation by modeling each time point as an IVP. As the IVP solvers are invertible by design, we propose to use the same IVP solver in the encoder and decoder of a VAE.

## 3 Methodology

In this section, we first formulate the problem, followed by a brief background on continuous-time models. We then introduce and describe our model in detail.

### 3.1 Problem Formulation

In our setup, we consider a multivariate time series  $X$  as a sequence of  $L$  observations:  $X = \{(\mathbf{x}_i, t_i)\}_{i=1}^L$ . Each observation  $\mathbf{x}_i$  is collected at a time  $t_i$ .  $\mathbf{x}_i \in \mathbf{R}^D$  where  $D$  represents the number of variables being measured at each time point (e.g., in EHR data these could represent a patient's heart rate, respiratory rate etc.). The dataset  $\mathcal{X}$  consists of  $N$  such sequences,  $\mathcal{X} = \{X_1, \dots, X_N\}$  collected within a fixed time window. Note that the length  $L$  of the sequences can vary across the dataset owing to the irregular spacing of the observation time points.

Our goal is to first build a generative model  $g$  for irregularly sampled time series (like EHR), which is capable of forecasting future values, and additionally augment it with a classifier to conduct classification tasks for which  $g$  serves as a representation learning module. The time series forecasting task is to predict observations  $X^\tau$  collected in time window  $[T, T + \tau]$ , based on past observations  $X$ , where  $\tau$  is the forecast horizon. The classification task is to predict the categorical label  $y$  of the sample  $X$ .

### 3.2 Continuous-time models

A continuous-time model [6] assumes that the data  $\mathbf{x}_t$  at time  $t$  is generated by a latent process  $F$  whose state  $\mathbf{z}$  can be propagated continuously to serve diverse purposes, such as generative modeling or representation learning. The propagation is achieved by solving IVPs, which are ordinary differential equations together with initial

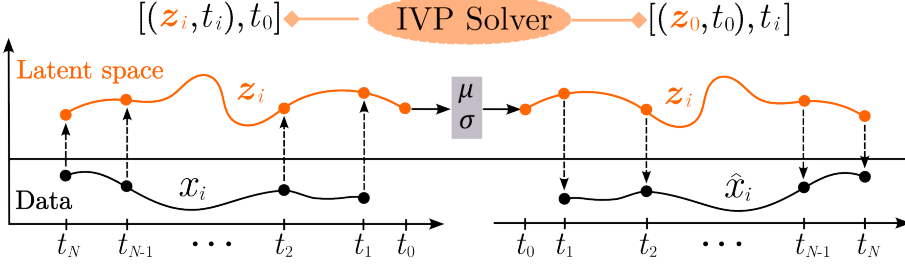


**Figure 2:** Modeling irregular time series with IVP-VAE. (Left) In the encoder, an embedding module maps data  $\mathbf{x}_i$  into latent state  $\mathbf{z}_i$ . The state is evolved backward in time: Take  $(\mathbf{z}_i, t_i)$  as initial condition and calculate state  $\mathbf{z}_0$  at  $t_0$  using an IVP solver. (Right) In the decoder, the latent state is evolved forward in time: Take  $(\mathbf{z}_0, t_0)$  as initial condition and go opposite along the timeline to obtain state  $\mathbf{z}_i$  using the same IVP solver. A reconstruction module then maps  $\mathbf{z}_i$  back to data  $\hat{\mathbf{x}}_i$ .

conditions, i.e.

$$F(t_0) = \mathbf{z}_0 \quad (1)$$

$$f(t, \mathbf{z}_t) = \frac{dF(t)}{dt} \quad (2)$$

$$\mathbf{z}_i = \mathbf{z}_{i-1} + \int_{t_{i-1}}^{t_i} f(t, \mathbf{z}_t) dt \quad (3)$$

Neural ODEs [6] parameterize  $f$  with uniformly Lipschitz continuous neural networks, which are used to specify the derivative at every  $t \in [t_0, T]$ . States of the continuous process were calculated using the Runge–Kutta method or other numeric integrators. Neural Flow [3] proposes to directly model the solution curve  $F$  with invertible neural networks. Both Neural ODEs and Neural Flow propagate hidden states by solving IVPs.

These continuous-time models are combined with recurrent units to analyze irregular time series. Given a hidden state  $\mathbf{z}_{i-1}$ , the idea to obtain the next hidden state is to propagate  $\mathbf{z}$  using an IVP solver until the next observation  $\mathbf{x}_i$  at time  $t_i$  and then to use an RNN cell to update it, as expressed by the following equations.

$$\mathbf{z}_i^- = \text{IVPSolve}((\mathbf{z}_{i-1}, t_{i-1}), t_i) \quad (4)$$

$$\mathbf{z}_i = \text{RNN}(\mathbf{x}_t, \mathbf{z}_i^-) \quad (5)$$

This represents the general IVP-RNN hybrid model first proposed in [27] using Neural ODEs as the IVP solver, known as Latent-ODE. A variant of Latent-ODE uses Neural Flow as the IVP solver to directly obtain  $\mathbf{z}_i^-$ , which we refer to as Latent-Flow in this paper. The entire model is trained as a VAE with the IVP-RNN hybrid model used as encoder to infer the posterior. Both Latent-ODE and Latent-Flow have proven to be effective in modeling irregular time series. However, the sequential nature of processing information makes these models computationally less efficient.

### 3.3 Proposed model: IVP-VAE

The key idea that our model builds upon is that time series values  $\{\mathbf{x}_i\}_{i=1}^L$  are discrete observations of an unknown continuous process. Each sample  $X$  correspondingly represents a continuous process, of which we obtain an indirect observation at each available timestamp  $t_i$ . In this sense, our proposed model IVP-VAE is essentially a generative model for these continuous processes. From this idea, we design the model following two basic points: (i) we can circumvent the sequential operation bottleneck by processing all time steps independently as one ODE’s different IVPs which can be solved in parallel. (ii) IVP solvers are inherently invertible, which enables us to use the same solver

for both forward and backward propagation. The model is trained as a VAE whose encoder includes an embedding module and the IVP solver evolving latent state  $\mathbf{z}_i$  backward in time, while the decoder includes the same IVP solver evolving the state forward in time, and a reconstruction module generating estimated data  $\hat{\mathbf{x}}_i$  based on state  $\mathbf{z}_i$ . The model is illustrated in Figure 2 and the whole idea is summarized in Algorithm 1. The steps are described in the following sections. The IVP-VAE model can then be used for different downstream tasks, for example by appending a classification module.

**Algorithm 1** IVP-VAE. The same IVP solver (highlighted in orange) works for both encoder and decoder by solving IVPs in opposite directions (highlighted in blue).

**Input:** Data points and timestamps  $X = \{(\mathbf{x}_i, t_i)\}_{i=1}^L$

**Output:** Reconstructed  $\{\hat{\mathbf{x}}_i\}_{i=1}^L$

- 1:  $t_0 = 0$
- 2:  $\{\mathbf{z}_i\}_{i=1}^L = \text{Embedding}(\{\mathbf{x}_i\}_{i=1}^L)$
- 3:  $\{\Delta t_i\}_{i=1}^L = t_0 - \{t_i\}_{i=1}^L$
- 4:  $\{\mathbf{z}_0\}_{i=1}^L = \text{IVPSolve}(\{\mathbf{z}_i, \Delta t_i\}_{i=1}^L)$
- 5:  $q(\mathbf{z}_0|X) = \text{Inference}(\{\mathbf{z}_0\}_{i=1}^L)$
- 6:  $\mathbf{z}_0 \sim q(\mathbf{z}_0|X)$
- 7:  $\{\Delta t_i\}_{i=1}^L = \{t_i\}_{i=1}^L - t_0$
- 8:  $\{\mathbf{z}_i\}_{i=1}^L = \text{IVPSolve}(\{\mathbf{z}_0, \Delta t_i\}_{i=1}^L)$
- 9:  $\{\hat{\mathbf{x}}_i\}_{i=1}^L = \text{Reconstruct}(\{\mathbf{z}_i\}_{i=1}^L)$
- 10: **return**  $\{\hat{\mathbf{x}}_i\}_{i=1}^L$

#### 3.3.1 Embedding and reconstruction

Within the embedding module, given a time series  $X = \{(\mathbf{x}_i, t_i)\}_{i=1}^L$ , we first generate corresponding binary masks  $\{\mathbf{m}_i\}_{i=1}^L$  that indicate which variables are observed and which are not at time  $t_i$ . Next, we obtain  $\mathbf{v}_i = (\mathbf{x}_i | \mathbf{m}_i)$  for all observations at  $t_i$  by concatenating  $\mathbf{x}_i$  with  $\mathbf{m}_i$ . A neural network  $\epsilon$  is then deployed on  $\mathbf{v}_i$ ,  $\mathbf{z}_i = \epsilon(\mathbf{v}_i)$ , to extract useful information from multivariate observations at each timestamp, and produce  $\mathbf{z}_i$  which represents the state of the continuous process at  $t_i$ .

On the decoder side, we design a similar module for data reconstruction that maps  $\mathbf{z}_i$  to  $\mathbf{x}_i$ . The aim of adding embedding and reconstruction modules is to create a space in which the latent state  $\mathbf{z}$  evolves, and also re-organize information into a more compact form. For those two modules, we use MLPs for demonstration and brevity.

They can be more complex or well-designed networks. The embedding and the reconstruction operation are respectively represented by line 2 and line 9 in Algorithm 1.

### 3.3.2 Evolving backward in time

Given that the true posterior  $p(\mathbf{z}_0 | X)$  is intractable [18], the overall goal is to approximate the posterior, i.e., learn a variational approximation  $q_\phi(\mathbf{z}_0 | X)$  which can then be used to sample  $\mathbf{z}_0$ . For  $\mathbf{x}_i$ , the initial condition is defined as  $(\mathbf{z}_i, t_i)$  in the encoder. The task of a neural IVP solver is to start from  $t_i$ , move towards  $t_0$  continuously and calculate  $\mathbf{z}_0$ :

$$\mathbf{z}_0^i = \text{IVPSolve}(\mathbf{z}_i, \Delta t_i), \quad (6)$$

where  $\Delta t_i = t_0 - t_i$ .  $(\mathbf{z}_i, t_i)$  and  $(\mathbf{z}_0^i, t_0)$  are on the same integral curve and satisfy the same ODE. Similarly,  $\{\mathbf{z}_0^i\}_{i=1}^L$  is obtained for all  $\{\mathbf{x}_i, \Delta t_i\}_{i=1}^L$ . As we take observation  $\mathbf{x}_i$  as an indirect observation of the unknown continuous process, we can make a guess of this process based on each  $\mathbf{x}_i$ , and then derive  $\mathbf{z}_0^i$  of the process. Here,  $\mathbf{z}_0^i$  is an estimation of  $\mathbf{z}_0$  made by the IVP solver based on  $\mathbf{x}_i$ . Afterward, there are two issues to be addressed. First, each  $\mathbf{z}_0^i$  should approximate  $\mathbf{z}_0$  during training. Second, all  $L \mathbf{z}_0^i$  should be integrated together for the following generative module (decoder). For the first issue, we will discuss more details in Section 3.4. For the second issue, we define  $q_\phi(\mathbf{z}_0 | X)$  to be the posterior distribution over the latent variable  $\mathbf{z}_0$  induced by the input time series  $X$ . To obtain it from  $\{q_\phi(\mathbf{z}_0^i | X)\}_{i=1}^L$  in Inference (line 5 in Algorithm 1), we introduce a mixture distribution over  $\{\mathbf{z}_0^i\}_{i=1}^L$ , constructed by diagonal Gaussian distribution  $\mathcal{N}$

$$q_\phi(\mathbf{z}_0^i | X) = \mathcal{N}(\boldsymbol{\mu}_{\mathbf{z}_0^i}, \boldsymbol{\sigma}_{\mathbf{z}_0^i}) \quad (7)$$

$$q_\phi(\mathbf{z}_0 | X) = \sum_{i=1}^L \pi_i * q_\phi(\mathbf{z}_0^i | X), \quad (8)$$

where  $\boldsymbol{\mu}_{\mathbf{z}_0^i} = h(\mathbf{z}_0^i)$ , and  $\boldsymbol{\sigma}_{\mathbf{z}_0^i} = \text{Softplus}(h(\mathbf{z}_0^i))$ .  $h$  denotes a feed-forward neural network and Softplus is the activation function.  $\pi$  denote the mixing coefficients for the  $L$  components. The entire operation is summarized by lines 3–5 in Algorithm 1. More details about  $\pi$  will be discussed in Section 3.4.2.

### 3.3.3 Evolving forward in time

In this part, we first draw an instance from the posterior distribution  $q_\phi(\mathbf{z}_0 | X)$  to obtain  $\mathbf{z}_0$  (line 6 in Algorithm 1), which will further be used as a representation of the time series sample and also as the initial point of extrapolation. We then start from  $\mathbf{z}_0$  and propagate the latent state  $\mathbf{z}$  forward along the timeline, with  $\Delta t_i = t_i - t_0$  (line 7). Thus,  $\mathbf{z}_1, \mathbf{z}_2, \dots, \mathbf{z}_L$  can be calculated for all the  $L$  timestamps by another call of the IVP solver (line 8):

$$\{\mathbf{z}_i\}_{i=1}^L = \text{IVPSolve}(\{\mathbf{z}_0, \Delta t_i\}_{i=1}^L). \quad (9)$$

The multivariate observation  $\mathbf{x}_i$  can then be obtained from  $\mathbf{z}_i$  using the data reconstruction module explained in section 3.3.1 (line 9 in Algorithm 1). The entire operation is mathematically represented as approximating  $p_\theta(X | z_0)$ .

In terms of capturing temporal dependencies, RNN-related models repeatedly operate on sequential observations and extract useful information in an autoregressive way. Using IVP-VAE, the dependence is captured by Neural ODEs with derivatives, and Neural Flows

with invertible transformations. Thus, the encoder and decoder do not require any recurrent operation, as all latent states at different time points can evolve independently given an ODE.

### 3.3.4 Invertibility and Bidirectional Evolving

The mechanism that one neural IVP solver works for both the encoder and decoder by solving IVPs in opposite time directions is achieved by utilizing the invertibility of IVP solvers. As for Neural ODEs, the state  $\mathbf{z}$  at different timestamps can be computed according to  $\mathbf{z}_i = \mathbf{z}_{i-1} + \int_{t_{i-1}}^{t_i} f(t, \mathbf{z}_t) dt$ , where  $f$  is determined within its domain of definition while  $\Delta t$  can be negative or positive. If positive, the state evolves forward in time. If negative, it evolves backward in time. Similarly, a flow  $\xi$  is mathematically defined as a group action on a set  $Z$  [2],

$$\xi : Z \times \mathbb{R} \rightarrow Z, \quad (10)$$

where for all  $\mathbf{z} \in Z$  and real number  $t$ ,

$$\xi(\mathbf{z}, 0) = \xi(\mathbf{z}), \quad (11)$$

$$\xi(\xi(\mathbf{z}, t_i), t_j) = \xi(\mathbf{z}, t_j + t_i). \quad (12)$$

This characteristic naturally guarantees its invertibility. And if  $t_j = -t_i$ , then  $\xi(\xi(\mathbf{z}, t_i), t_j) = \xi(\mathbf{z}, 0) = \xi(\mathbf{z})$  can describe the whole evolving process from encoder to decoder.

## 3.4 Training

The IVP-VAE model can be trained both on unsupervised and supervised learning.

### 3.4.1 Unsupervised Learning

To learn the parameters of our IVP-VAE model given a dataset of sparse and irregularly sampled time series, we define the learning objective for one sample  $X$  as

$$\begin{aligned} \mathcal{L}_{\text{VAE}}(\phi, \theta) = & \mathbb{E}_{\mathbf{z}_0 \sim q_\phi(\mathbf{z}_0 | X)} [\log p_\theta(X | \mathbf{z}_0)] \\ & - \frac{1}{L} \sum_{i=1}^L D_{KL}(q_\phi(\mathbf{z}_0^i | X) \| p(\mathbf{z}_0)), \end{aligned} \quad (13)$$

which corresponds to the evidence lower bound (ELBO) [18].

As mentioned earlier in Section 3.3.2, each  $\mathbf{z}_0^i$  should approximate  $\mathbf{z}_0$  during training, the second term of  $\mathcal{L}_{\text{VAE}}(\phi, \theta)$  is the average of KL-divergence loss between  $\{q_\phi(\mathbf{z}_0^i | X)\}_{i=1}^L$  and  $p(\mathbf{z}_0)$ . Given that not all data dimensions are observed at all time points, we calculate the reconstruction loss based on all available observations.

### 3.4.2 Supervised Learning

**Forecasting.** The model's capability of extrapolation can be used for time series forecasting. To produce value predictions out of the input time window  $T$ , one can simply continue to propagate the latent state  $\mathbf{z}_i$  using the same neural IVP solver to any desired time points, e.g. in the forecast time window  $[T, T + \tau]$ , without adding any additional component. After propagation, the same reconstruction module can be used to map  $\mathbf{z}_i$  to  $\hat{\mathbf{x}}_i$ , thus obtaining  $\hat{X}^\tau$ , which is the forecasted content with regard to the truth  $X^\tau$ . We combine  $\mathcal{L}_{\text{VAE}}$  with the reconstruction error  $\mathcal{L}_{\text{Re}}$  on  $X^\tau$  to obtain Equation 14, where  $\alpha$  is a hyperparameter.

$$\mathcal{L}_{\text{Forecast}}(\phi, \theta) = \mathcal{L}_{\text{VAE}}(\phi, \theta) + \alpha \cdot \mathcal{L}_{\text{Re}}(\hat{X}^\tau \| X^\tau) \quad (14)$$

**Classification.** We can also augment IVP-VAE with a classifier that leverages the latent state evolving as feature extraction and representation learning. We define this portable classification component to be of the form  $p_\lambda(y | \mathbf{z}_0)$ , where  $\lambda$  represents model parameters (essentially a feed-forward network). This leads to an augmented learning objective as shown in Equation 15, where CE represents the cross entropy loss.

$$\mathcal{L}_{\text{Class}}(\phi, \theta, \lambda) = \mathcal{L}_{\text{VAE}}(\phi, \theta) + \alpha \cdot \text{CE}(p(y) \| p_\lambda(y | \mathbf{z}_0)) \quad (15)$$

The value of the mixing coefficient  $\pi_i$  in Equation 8 depends on the performed task. There exist various methods to determine the mixing coefficients in a mixture distribution. In our proposed model, we empirically obtained two different settings for the mixing coefficients:  $\pi_i = \frac{1}{L}$  for classification tasks and  $\pi_i = \frac{D_{KL}(q_\phi(\mathbf{z}_0^i | \mathbf{X}) \| p(\mathbf{z}_0))}{\sum_{j=1}^L D_{KL}(q_\phi(\mathbf{z}_0^j | \mathbf{X}) \| p(\mathbf{z}_0))}$  for forecasting tasks.

## 4 Experiments

In this section, we evaluate IVP-VAE’s capability of data modeling and representation learning for EHR time series data. We present forecasting and classification experiments using a range of baseline models and EHR datasets.

### 4.1 Datasets

We evaluate our model on three real-world public EHR datasets from the PhysioNet platform [11]: MIMIC-IV [14, 15], PhysioNet 2012 [32] and eICU [23, 24].

The **MIMIC-IV** dataset is a multivariate EHR time series dataset consisting of sparse and irregularly sampled physiological signals collected at Beth Israel Deaconess Medical Center from 2008 to 2019. After data preprocessing following a similar procedure to [3], 96 variables covering patient in- and outputs, laboratory measurements, and prescribed medications, are extracted over the first 48 hours after ICU admission. We obtain 26,070 records and use them for both forecasting and classification.

The **PhysioNet 2012** dataset was published as part of the PhysioNet/Computing in Cardiology Challenge 2012 with the objective of in-hospital mortality prediction. It includes vital signs, laboratory results, and demographics of patients admitted to an ICU. We use the provided 4,000 admissions from the challenge training set and 41 features over the first 48 hours after patient admission following [3].

The **eICU** Collaborative Research Database is a multi-center dataset of patients admitted to ICUs at 208 hospitals located throughout the United States between 2014 and 2015. We follow the preprocessing procedure presented in [26] and extract 14 features over the first 48 hours after ICU admission for 12,312 admissions.

The key information of the three datasets after preprocessing is summarized in Table 1. MIMIC-IV has the highest rate of missing values, the longest average sequence length, and the smallest positive rate for mortality. The eICU data are the least sparse, with a missing rate of only about 65 %. The full list of selected variables of each dataset can be found in Appendix 6.2.

### 4.2 Baselines

We compare our model against several baselines for the forecasting and classification of multivariate irregular time-series.

- **GRU- $\Delta_t$**  concatenates feature values with masking variable and time interval  $\Delta_t$  as input [27].

**Table 1:** Key information of the three datasets after preprocessing: Number of admissions used, number of selected variables, overall percentage of missing values, average sequence length over admissions, positive rate for mortality, granularity of measurements.

	MIMIC-IV	PhysioNet 2012	eICU
# Samples	26,070	3,989	12,312
# Variables	96	41	14
Missing rate (%)	97.95	85.74	65.25
Average length	173.4	75.0	114.55
Positive rate (%)	13.39	13.89	17.61
Granularity	1 min	1 min	1 min

- **GRU-D** incorporates missing patterns using GRU combined with a learnable decay mechanism on both the input sequence and hidden states [5].
- **mTAN** leverages an attention mechanism to learn temporal similarity and time embeddings [31].
- **GRU-ODE-Bayes** couples continuous-time ODE dynamics with discrete Bayesian update steps [8].
- **CRU** constructs continuous recurrent cells using linear stochastic differential equations and Kalman filters [28].
- **Raindrop** represents dependencies among multivariate with a graph whose connectivity is learned from time series [37].
- **Latent-ODE** uses an ODE-RNN encoder and Neural ODE decoder in a VAE architecture [27].
- **Latent-Flow** replaces the ODE component of Latent-ODE with more efficient Neural Flow models [3].

Corresponding to two Latent-based models, we evaluate IVP-VAE with two types of IVP solvers, i.e. one with ODE called IVP-VAE-ODE and another with Flow called IVP-VAE-Flow. Hyperparameter settings are described in Appendix 6.1. Latent-ODE and Latent-Flow, which are the primary baselines for our model, are jointly referred to as *latent-based* models in this section.

### 4.3 Experimental Protocols

All three datasets are used for forecasting and classification experiments, and each of them contains 48 hours of observation after ICU admission. Each dataset is randomly split into 80% for training, 10% for validation and 10% for testing. We repeat each experiment five times using different random seeds to split datasets and initialize model parameters.

In forecasting experiments, we use the first 24 hours of data as input and prediction the next 24 hours of data. We assess models’ performance using the mean squared error (MSE). While for classification experiments, we focus on predicting in-hospital mortality using the first 24 hours of data. Due to class imbalance in these datasets, we assess classification performance using area under the ROC curve (AUROC) and area under the precision-recall curve (AUPRC). To compare the models’ running speed, we also report T-epoch [3, 13, 31], which is the time that each model needs to complete one epoch (counted in seconds). All models were tested in the same computing environment with NVIDIA Tesla V100 GPUs.

With regard to “Granularity” in Table 1, all models are trained and tested with a granularity of 1 min, except for Raindrop which consumes too much GPU memory when sequences are long and variables are many. For Raindrop, to load the model and data into GPUs, we increase the granularity to 5 min on PhysioNet 2012 and 10 min on MIMIC-IV, by merging accumulated measurements within the new granularity.

**Table 2:** Test MSE (lower is better) and time per epoch in seconds (T-epoch) for forecasting on datasets MIMIC-IV, PhysioNet 2012, and eICU. Top two results are shown in **bold**. IVP-VAE-based models achieved comparable results among all baselines and are multiple times faster than their Latent-based counterparts.

	MIMIC-IV		PhysioNet 2012		eICU	
	MSE	T-epoch	MSE	T-epoch	MSE	T-epoch
GRU- $\Delta_t$	0.730 $\pm$ 0.014	615.3	0.567 $\pm$ 0.012	78.6	0.583 $\pm$ 0.009	119.0
GRU-D	0.736 $\pm$ 0.005	727.3	0.579 $\pm$ 0.014	84.8	<b>0.578<math>\pm</math>0.007</b>	150.3
GOB	0.809 $\pm$ 0.014	5445.3	0.613 $\pm$ 0.007	339.5	0.664 $\pm$ 0.012	1699.6
mTAN	<b>0.716<math>\pm</math>0.011</b>	114.6	0.576 $\pm$ 0.018	7.6	0.582 $\pm$ 0.010	27.9
CRU	0.946 $\pm$ 0.016	1262.6	0.687 $\pm$ 0.030	73.1	0.820 $\pm$ 0.044	373.6
Latent-ODE	0.769 $\pm$ 0.024	4294.9	0.615 $\pm$ 0.035	394.7	0.598 $\pm$ 0.005	1432.0
Latent-Flow	0.755 $\pm$ 0.011	2272.0	0.612 $\pm$ 0.037	228.3	0.594 $\pm$ 0.007	569.6
IVP-VAE-ODE	<b>0.724<math>\pm</math>0.011</b>	155.4	<b>0.552<math>\pm</math>0.007</b>	23.6	0.596 $\pm$ 0.018	83.2
IVP-VAE-Flow	0.727 $\pm$ 0.013	81.5	<b>0.553<math>\pm</math>0.007</b>	8.6	<b>0.581<math>\pm</math>0.009</b>	28.0

**Table 3:** Test AUROC and AUPRC (higher is better) for mortality prediction on three datasets. We additionally report the time per epoch in seconds (T-epoch). IVP-VAE-based models obtain comparable results and are multiple times faster than Latent-based models.

	MIMIC-IV			PhysioNet 2012			eICU		
	AUROC	AUPRC	T-epoch	AUROC	AUPRC	T-epoch	AUROC	AUPRC	T-epoch
GRU- $\Delta_t$	<b>0.809<math>\pm</math>0.006</b>	0.420 $\pm$ 0.020	1464.8	0.733 $\pm$ 0.040	0.292 $\pm$ 0.036	27.0	0.761 $\pm$ 0.014	0.428 $\pm$ 0.021	321.8
GRU-D	0.786 $\pm$ 0.009	0.419 $\pm$ 0.013	1794.7	0.754 $\pm$ 0.029	0.319 $\pm$ 0.034	32.1	<b>0.796<math>\pm</math>0.015</b>	<b>0.477<math>\pm</math>0.024</b>	347.9
mTAN	0.766 $\pm$ 0.006	0.379 $\pm$ 0.024	1447.2	0.746 $\pm$ 0.032	0.318 $\pm$ 0.029	27.3	0.769 $\pm$ 0.024	0.451 $\pm$ 0.032	321.3
Raindrop	0.774 $\pm$ 0.004	0.373 $\pm$ 0.021	1152.8	0.768 $\pm$ 0.025	0.332 $\pm$ 0.032	36.0	0.766 $\pm$ 0.021	0.451 $\pm$ 0.027	323.2
Latent-ODE	0.768 $\pm$ 0.008	0.393 $\pm$ 0.002	5270.3	0.770 $\pm$ 0.025	0.343 $\pm$ 0.039	363.8	0.783 $\pm$ 0.018	<b>0.477<math>\pm</math>0.024</b>	1577.9
Latent-Flow	0.786 $\pm$ 0.007	0.404 $\pm$ 0.025	3105.5	<b>0.774<math>\pm</math>0.019</b>	0.352 $\pm$ 0.023	207.7	0.781 $\pm$ 0.020	<b>0.482<math>\pm</math>0.029</b>	776.5
IVP-VAE-ODE	0.802 $\pm$ 0.011	<b>0.422<math>\pm</math>0.014</b>	1478.8	<b>0.783<math>\pm</math>0.026</b>	<b>0.377<math>\pm</math>0.051</b>	34.4	0.786 $\pm$ 0.014	0.468 $\pm$ 0.026	348.4
IVP-VAE-Flow	<b>0.805<math>\pm</math>0.005</b>	<b>0.427<math>\pm</math>0.014</b>	1445.8	0.770 $\pm$ 0.024	<b>0.390<math>\pm</math>0.029</b>	32.9	<b>0.786<math>\pm</math>0.017</b>	0.472 $\pm$ 0.029	323.3

Considering the fact that even though some public EHR datasets have sufficient general samples for training complex deep learning models, when it comes to a specific group of patients or a specific medical phenomenon, the available data for training are usually not sufficient [29]. We also deploy our model and other baselines on experiments with limited samples. To simulate the challenge, we created 3 small datasets by randomly drawing 250, 500, and 1,000 samples from the MIMIC IV dataset. These samples are used for training and validation by the rate 4:1. We then draw 2,000 samples from the rest of the dataset to construct an independent testing set. Both classification and forecasting tasks are also deployed in this setting.

#### 4.4 Results and Analyses

We analyze the results of IVP-VAE for forecasting and classification experiments, its efficiency, and the performance on small datasets.

##### 4.4.1 Forecasting Experiments

The results of forecasting experiments on the three datasets are shown in Table 2. For each metric, we use bold font to indicate the best two results.

Both ODE and Flow versions of IVP-VAE consistently outperform the state-of-the-art latent continuous time models across the three datasets. When compared with other state-of-the-art baseline models, IVP-VAE achieves at least the second-best result, even achieving the best result for the PhysioNet 2012 dataset. Overall, our proposed methods IVP-VAE-Flow and IVP-VAE-ODE exhibit competitive performance across all the datasets.

With respect to efficiency (measured in terms of T-epoch, i.e., time required to complete 1 epoch), the proposed IVP-VAE models achieve

a significant speedup (as high as 25x on MIMIC-IV) over their latent-based counterparts. Among the other baseline models, only mTAN has a lower T-epoch value compared to the IVP-VAE models. However, the difference is significant only for PhysioNet 2012 dataset where the time series are comparatively shorter as noted in Table 1. We attribute this drop in efficiency of mTAN to the use of bidirectional RNNs, which are slower for longer sequences [31].

##### 4.4.2 Classification Experiments

The performance of the models on the classification task in terms of AUROC and AUPRC across the three datasets is reported in Table 3. With respect to the latent-based counterparts, IVP-VAE models achieve comparable result and at the same time achieve significant speedup. The proposed models also outperform most of the other baseline models for MIMIC-IV and PhysioNet 2012 datasets.

Overall, we note the proposed models to be more advantageous for MIMIC IV and PhysioNet 2012 datasets. This can perhaps be attributed to the number of variables and the sparsity of the data. In comparison, the eICU dataset has fewer variables and a lower missing rate. For both IVP-VAE and Latent-based models, we further note that Flow variants mostly outperform the ODE variants across the datasets and tasks. We speculate this to be because of neural ODEs capturing the temporal evolving patterns with only first order ODEs. On the other hand, Neural Flows can capture more complex patterns that are governed by higher order ODEs.

##### 4.4.3 Efficiency Improvement

To have a clear view of the efficiency improvement of our models compared to Latent-based models, we make a detailed comparison of these two types on MIMIC-IV dataset in Table 5.

**Table 4:** Experiment results on small datasets of MIMIC-IV for 250, 500 and 1000 admissions selected for training and validation, respectively. Test AUROC (higher is better) is shown for classification and MSE (lower is better) for the forecasting task. IVP-VAE models outperform the baselines in both forecast and classification tasks across all small dataset settings.

	250		500		1000	
	AUROC	MSE	AUROC	MSE	AUROC	MSE
GRU- $\Delta_t$	0.600 $\pm$ 0.016	0.893 $\pm$ 0.015	0.676 $\pm$ 0.017	0.902 $\pm$ 0.056	0.733 $\pm$ 0.010	0.823 $\pm$ 0.018
GRU-D	0.610 $\pm$ 0.018	0.893 $\pm$ 0.020	0.652 $\pm$ 0.027	0.861 $\pm$ 0.021	0.709 $\pm$ 0.025	0.807 $\pm$ 0.014
mTAN	0.683 $\pm$ 0.036	0.956 $\pm$ 0.031	0.716 $\pm$ 0.009	0.908 $\pm$ 0.025	0.723 $\pm$ 0.023	0.850 $\pm$ 0.044
GRU-ODE-Bayes	-	0.882 $\pm$ 0.021	-	0.877 $\pm$ 0.018	-	0.846 $\pm$ 0.023
CRU	-	0.938 $\pm$ 0.053	-	0.898 $\pm$ 0.015	-	0.872 $\pm$ 0.013
Raindrop	0.637 $\pm$ 0.038	-	0.710 $\pm$ 0.036	-	0.737 $\pm$ 0.011	-
Latent-ODE	0.667 $\pm$ 0.045	1.028 $\pm$ 0.048	0.693 $\pm$ 0.029	1.042 $\pm$ 0.033	0.707 $\pm$ 0.029	1.028 $\pm$ 0.082
Latent-Flow	0.686 $\pm$ 0.011	1.046 $\pm$ 0.044	0.694 $\pm$ 0.031	1.080 $\pm$ 0.136	0.715 $\pm$ 0.054	1.046 $\pm$ 0.078
IVP-VAE-ODE	0.714 $\pm$ 0.009	0.869 $\pm$ 0.032	<b>0.736<math>\pm</math>0.025</b>	0.825 $\pm$ 0.020	0.758 $\pm$ 0.025	0.776 $\pm$ 0.028
IVP-VAE-Flow	<b>0.718<math>\pm</math>0.010</b>	<b>0.865<math>\pm</math>0.022</b>	0.735 $\pm$ 0.029	<b>0.813<math>\pm</math>0.017</b>	<b>0.760<math>\pm</math>0.015</b>	<b>0.766<math>\pm</math>0.030</b>

- dash denotes that the model does not support this task

Efficiency is measured in terms of T-epoch and T-forward (the time taken by each model to complete one forward run). Clearly, IVP-VAE models are able to achieve a significant speed advantage over the corresponding Latent-based models. For instance, on forecasting tasks, IVP-VAE-Flow is about 42 times faster than Latent-Flow in terms of T-forward. Given, T-epoch includes T-forward, as well as time for data loading, loss calculation, backpropagation, etc., which significantly contributes to the computation time, the improvement in T-epoch is not as significant as in T-forward. Nevertheless, IVP-VAE-Flow is still more than 28 times faster than Latent-Flow. The speed advantage is achieved by eliminating recurrent operations and solving IVPs in parallel.

Furthermore, we compare IVP-VAE with its counterparts on convergence rate. As shown in Table 5, IVP-VAE models converge significantly faster than Latent-based models, with IVP-VAE models needing lesser epochs to achieve the best validation accuracy. This advantage is achieved by the parameter sharing mechanism in our models, i.e. one IVP solver for both the encoder and decoder. Multiplying the time per epoch by the number of epochs to obtain the total training time, we find that IVP-VAE based models are at least one order of magnitude faster than Latent-based models for both classification and forecasting tasks.

Regarding model size (# Parameters in Table 5), IVP-VAE-ODE is little larger than Latent-ODE, and IVP-VAE-Flow is smaller than Latent-Flow. To figure out the inconsistency, we need to note that compared with Latent-based models, IVP-VAE (1) eliminates recurrent units, (2) uses one IVP solver rather than two, and (3) adds in the embedding and reconstruction modules. Factor (1) and (2) can reduce the number of parameters, while factor (3) increases the number of parameters. As Neural Flows have more parameters than Neural ODEs, the "one IVP solver for both encoder and decoder" mechanism makes a larger contribution for IVP-VAE-Flow with regard to reducing parameters.

#### 4.4.4 Experiments on Small Datasets

To further demonstrate proposed models' capabilities, we examine its performance under conditions of low sample size. This scenario is analogous to a rare disease setup in the field of EHR prediction, where data can be obtained for only a few patients. In such cases, models' effectiveness in comprehending temporal evolving patterns and rapidly updating parameters becomes essential.

Table 4 compares the performance of all methods on small datasets where we only collected limited number of samples for model training

**Table 5:** Comparison of the efficiency of IVP-VAE and Latent-based models on the MIMIC-IV dataset. We compare the time needed for one forward pass (T-forward), time needed for one epoch (T-epoch), number of epochs and number of parameters.

		IVP-VAE		Latent-based	
		ODE	Flow	ODE	Flow
Classification	T-forward	0.066	0.017	2.536	0.784
	T-epoch	1478.8	1445.8	5270.3	3105.5
	# Epochs	12.6	10.8	56.2	57.8
	# Parameters	209,677	325,017	199,017	429,697
Forecasting	T-forward	0.106	0.025	3.059	1.063
	T-epoch	155.4	81.5	4294.9	2272.0
	# Epochs	23.4	30.2	42.6	51.0
	# Parameters	112,776	228,116	102,116	332,796

and validation. As we can see, on both forecast and classification tasks, IVP-VAE based models consistently and substantially outperforms all the baseline approaches across all settings of collected samples. The advantage of the model on small datasets is also due to its parameter sharing mechanism in the encoder and decoder.

## 5 Conclusion and Discussion

In this paper, we have presented a faster and lighter continuous-time generative model IVP-VAE, which is able to model and learn representation of irregular sampled EHR time series by purely solving IVPs in parallel under the VAE architecture. Our results showed that the proposed models perform comparable or better than other baselines on classification and forecasting tasks, while offering training time that is one order of magnitude faster than previous continuous-time methods. Further experiments on small datasets showed that our model has an advantage in scenarios where the number of training samples is limited. Based on this, more work can be done on demonstrating IVP-VAE's capability of modeling irregular sample time series with diverse datasets, not only EHR datasets, and different tasks like missing value imputation, time series regression, etc.

## Acknowledgements

This research was funded by the Federal Ministry of Education and Research (BMBF), Germany under the project LeibnizKILabor with grant No. 01DD20003.

## References

- [1] Noura S Abul-Husn and Eimear E Kenny, ‘Personalized medicine and the power of electronic health records’, *Cell*, **177**(1), 58–69, (2019).
- [2] Nam Parshad Bhatia and Giorgio P. Szegö, *Stability theory of dynamical systems*, volume 31, 5–6, Springer Science & Business Media, first edn., 1970.
- [3] Marin Biloš, Johanna Sommer, Syama Sundar Rangapuram, Tim Januschowski, and Stephan Günnemann, ‘Neural flows: Efficient alternative to neural ODEs’, *Advances in neural information processing systems*, **32**, (2021).
- [4] Wei Cao, Dong Wang, Jian Li, Hao Zhou, Lei Li, and Yitan Li, ‘BRITS: Bidirectional recurrent imputation for time series’, *Advances in neural information processing systems*, **31**, (2018).
- [5] Zhengping Che, Sanjay Purushotham, Kyunghyun Cho, David Sontag, and Yan Liu, ‘Recurrent neural networks for multivariate time series with missing values’, *Scientific Reports*, **8**, 1–12, (2018).
- [6] Ricky T. Q. Chen, Yulia Rubanova, Jesse Bettencourt, and David K. Duvenaud, ‘Neural ordinary differential equations’, *Advances in Neural Information Processing Systems*, **31**, (2018).
- [7] Jen-Tzung Chien and Yi-Hsiang Chen, ‘Continuous-time attention for sequential learning’, in *Proceedings of the AAAI Conference on Artificial Intelligence*, volume 35, pp. 7116–7124, (2021).
- [8] Edward De Brouwer, Jaak Simm, Adam Arany, and Yves Moreau, ‘GRU-ODE-Bayes: Continuous modeling of sporadically-observed time series’, *Advances in neural information processing systems*, **32**, (2019).
- [9] Matthias Fey, Jan Eric Lenssen, Frank Weichert, and Heinrich Müller, ‘SplineCNN: Fast geometric deep learning with continuous B-spline kernels’, in *Proceedings of the IEEE conference on computer vision and pattern recognition*, pp. 869–877, (2018).
- [10] Yue Gao, Guang-Yao Cai, Wei Fang, Hua-Yi Li, Si-Yuan Wang, Lingxi Chen, Yang Yu, Dan Liu, Sen Xu, Peng-Fei Cui, et al., ‘Machine learning based early warning system enables accurate mortality risk prediction for covid-19’, *Nature communications*, **11**(1), 5033, (2020).
- [11] Ary L. Goldberger, Luis A. N. Amaral, Leon Glass, Jeffrey M. Hausdorff, Plamen Ch. Ivanov, Roger G. Mark, Joseph E. Mietus, George B. Moody, Chung-Kang Peng, and H. Eugene Stanley, ‘PhysioBank, PhysioToolkit, and PhysioNet’, *Circulation*, **101**, (2000).
- [12] Hravir Harutyunyan, Hrant Khachatrian, David C Kale, Greg Ver Steeg, and Aram Galstyan, ‘Multitask learning and benchmarking with clinical time series data’, *Scientific data*, **6**(1), 96, (2019).
- [13] Max Horn, Michael Moor, Christian Bock, Bastian Rieck, and Karsten Borgwardt, ‘Set functions for time series’, in *International Conference on Machine Learning*, volume 119, pp. 4353–4363. PMLR, (2020).
- [14] Alistair E. W. Johnson, Lucas Bulgarelli, Tom J. Pollard, Steven Horng, Leo A. Celi, and Roger G. Mark. MIMIC-IV (version 1.0), 2020.
- [15] Alistair E. W. Johnson, Lucas Bulgarelli, Lu Shen, Alvin Gayles, Ayad Shamout, Steven Horng, Tom J. Pollard, Benjamin Moody, Brian Gow, Li-wei H. Lehman, Leo A. Celi, and Roger G. Mark, ‘MIMIC-IV, a freely accessible electronic health record dataset’, *Scientific Data*, **10**(1), 1–9, (2023).
- [16] Alistair E. W. Johnson, Tom J. Pollard, Lu Shen, Li wei H. Lehman, Mengling Feng, Mohammad Ghassemi, Benjamin Moody, Peter Szolovits, Leo A. Celi, and Roger G. Mark, ‘MIMIC-III, a freely accessible critical care database’, *Scientific Data*, **3**, 160035, (2016).
- [17] Yeo Jin Kim and Min Chi, ‘Temporal belief memory: imputing missing data during RNN training’, in *Proceedings of the 27th International Joint Conference on Artificial Intelligence*, pp. 2326–2332, (2018).
- [18] Diederik P. Kingma and Max Welling, ‘Auto-encoding variational Bayes’, in *International Conference on Learning Representations, ICLR*, (2014).
- [19] Qianting Li and Yong Xu, ‘VS-GRU: A variable sensitive gated recurrent neural network for multivariate time series with massive missing values’, *Applied Sciences*, **9**(15), (2019).
- [20] Steven Cheng-Xian Li and Benjamin M. Marlin, ‘Learning from irregularly-sampled time series: A missing data perspective’, in *International Conference on Machine Learning*, pp. 5937–5946. PMLR, (2020).
- [21] Zachary C Lipton, John Berkowitz, and Charles Elkan, ‘A critical review of recurrent neural networks for sequence learning’, *arXiv preprint arXiv:1506.00019*, (2015).
- [22] Matthew McDermott, Bret Nestor, Evan Kim, Wancong Zhang, Anna Goldenberg, Peter Szolovits, and Marzyeh Ghassemi, ‘A comprehensive ehr timeseries pre-training benchmark’, in *Proceedings of the Conference on Health, Inference, and Learning*, pp. 257–278, (2021).
- [23] Tom J. Pollard, Alistair E. W. Johnson, Jesse D. Raffa, Leo A. Celi, Omar Badawi, and Roger Mark. eICU Collaborative Research Database (version 2.0), 2019.
- [24] Tom J. Pollard, Alistair E. W. Johnson, Jesse D. Raffa, Leo A. Celi, Roger G. Mark, and Omar Badawi, ‘The eICU collaborative research database, a freely available multi-center database for critical care research’, *Scientific data*, **5**(1), 1–13, (2018).
- [25] Sanjay Purushotham, Chuizheng Meng, Zhengping Che, and Yan Liu, ‘Benchmarking deep learning models on large healthcare datasets’, *Journal of biomedical informatics*, **83**, 112–134, (2018).
- [26] David W. Romero, Anna Kuzina, Erik J. Bekkers, Jakub M. Tomczak, and Mark Hoogendoorn, ‘CKConv: Continuous kernel convolution for sequential data’, in *International Conference on Learning Representations (ICLR)*, (2022).
- [27] Yulia Rubanova, Ricky T. Q. Chen, and David Duvenaud, ‘Latent ODEs for irregularly-sampled time series’, *Advances in neural information processing systems*, **32**, (2019).
- [28] Mona Schirmer, Mazin Eltayeb, Stefan Lessmann, and Maja Rudolph, ‘Modeling irregular time series with continuous recurrent units’, in *International Conference on Machine Learning*, pp. 19388–19405. PMLR, (2022).
- [29] Benjamin Shickel, Patrick James Tighe, Azra Bihorac, and Parisa Rashidi, ‘Deep ehr: a survey of recent advances in deep learning techniques for electronic health record (ehr) analysis’, *IEEE journal of biomedical and health informatics*, **22**(5), 1589–1604, (2017).
- [30] Satya Narayan Shukla and Benjamin M. Marlin, ‘A survey on principles, models and methods for learning from irregularly sampled time series’, *NeurIPS 2020 Workshop: ML Retrospectives, Surveys & Meta-Analyses*, (11 2020).
- [31] Satya Narayan Shukla and Benjamin M. Marlin, ‘Multi-time attention networks for irregularly sampled time series’, in *International Conference on Learning Representations (ICLR)*, (2021).
- [32] Ikaro Silva, George Moody, Daniel J. Scott, Leo A. Celi, and Roger G. Mark, ‘Predicting in-hospital mortality of ICU patients: The PhysioNet/Computing in Cardiology Challenge 2012’, in *Computing in Cardiology*, volume 39, pp. 245–248, (2012).
- [33] Chenxi Sun, Shenda Hong, Moxian Song, and Hongyan Li, ‘A review of deep learning methods for irregularly sampled medical time series data’, *arXiv preprint arXiv:2010.12493*, (2020).
- [34] Mahanazuddin Syed, Shorabuddin Syed, Kevin Sexton, Hafsa Barea Syeda, Maryam Garza, Meredith Zozus, Farhanuddin Syed, Salma Begum, Abdullah Usama Syed, Joseph Sanford, and Fred Prior, ‘Application of machine learning in intensive care unit (ICU) settings using MIMIC dataset: Systematic review’, *Informatics*, **8**(1), 16, (2021).
- [35] Sindhu Tipirneni and Chandan K. Reddy, ‘Self-supervised transformer for sparse and irregularly sampled multivariate clinical time-series’, *ACM Transactions on Knowledge Discovery from Data (TKDD)*, **16**(6), 1–17, (2022).
- [36] Philip B. Weerakody, Kok Wai Wong, Guanjin Wang, and Wendell Ela, ‘A review of irregular time series data handling with gated recurrent neural networks’, *Neurocomputing*, **441**, 161–178, (2021).
- [37] Xiang Zhang, Marko Zeman, Theodoros Tsiligkaridis, and Marinka Zitnik, ‘Graph-guided network for irregularly sampled multivariate time series’, in *International Conference on Learning Representations (ICLR)*, (2022).
- [38] Haoyi Zhou, Shanghang Zhang, Jieqi Peng, Shuai Zhang, Jianxin Li, Hui Xiong, and Wancai Zhang, ‘Informer: Beyond efficient transformer for long sequence time-series forecasting’, in *Proceedings of the AAAI conference on artificial intelligence*, volume 35, pp. 11106–11115, (2021).

## 6 Appendix

### 6.1 Hyperparameter and detailed model settings

#### 6.1.1 All experiments

- Optimizer: Adam
- Weight decay: 1e-4
- Batch size: 50
- Learning rate: 1e-3
- Learning rate scheduler step: 20
- Learning rate decay: 0.5

#### 6.1.2 Model detailed settings

##### IVP-VAE

- Latent state dimension: 20
- $\alpha$  balancing the cross-entropy loss and ELBO
  - MIMIC-IV: 1000
  - PhysioNet 2012: 100
  - eICU: 100
- $\alpha$  balancing forecasting loss and ELBO: 1
- Variants
  - **IVP-VAE-Flow**
    - \* Flow model: ResNet flow
    - \* Number of flow layers: 2
  - **IVP-VAE-ODE**
    - \* Integrator: dopri5

##### Latent-based models

- Latent state dimension: 20
- $\alpha$  balancing the cross-entropy loss and ELBO: 100
- $\alpha$  balancing forecasting loss and ELBO: 1
- Variants
  - **Latent-Flow**
    - \* Flow model: ResNet flow
    - \* Number of flow layers: 2
  - **Latent-ODE**
    - \* Integrator: dopri5

##### RNN-based models

- Hidden dimension: 20
- Variants
  - **GRU- $\Delta_t$**
  - **GRU-D**

##### mTAN

- Hidden dimension: 20
- Hidden dimension of the recognition module: 256
- Hidden dimension of the generative module: 50
- Dimension of the embedded time feature: 128
- Number of attention heads: 1

- Number of reference points: 128
- $\alpha$  balancing the cross-entropy loss and ELBO: 100
- $\alpha$  balancing forecasting loss and ELBO: 1

##### Raindrop

- Dimension of the position encoder: 16
- Number of attention heads: 4
- Dropout rate: 0.2
- Number of Transformer Encoder layers: 2

##### CRU

- Number of hidden units: 50
- Number of basis matrices: 20
- Bandwidth for basis matrices: 10

##### GRU-ODE-Bayes

- Ratio between KL and update loss: 0.0001
- Size of hidden state for covariates: 10
- Size of hidden state for initialization: 25

### 6.2 Selected variables

For a summary of the variables selected for the MIMIC-IV, PhysioNet 2012 and eICU datasets, see Table 6.

**Table 6:** Selected variables for MIMIC-IV, PhysioNet 2012 and eICU dataset.

MIMIC-IV	PhysioNet 2012	eICU
Anion Gap	Age	HR
Bicarbonate	Gender	MAP
Calcium, Total	Height	Diast. BP
Chloride	ICUType	Syst. BP
Glucose	Weight	O2
Magnesium	Albumin	Resp
Phosphate	ALP	Temperature
Potassium	ALT	Glucose
Sodium	AST	FiO2
Alkaline Phosphatase	Bilirubin	pH
Aspartate Aminotransferase	BUN	Height
Bilirubin, Total	Cholesterol	Weight
Urea Nitrogen	Creatinine	Age
Basophils	DiasABP	Admission diagnosis
Eosinophils	FiO2	Gender
Hematocrit	GCS	Ethnicity
Hemoglobin	Glucose	Glasgow Coma Score Total
Lymphocytes	HCO3	GCS Eyes
MCH	HCT	GCS Motor
MCHC	HR	GCS Verbal
MCV	K	
Monocytes	Lactate	
Neutrophils	Mg	
Platelet Count	MAP	
RDW Piggyback	MechVent	
Red Blood Cells	Na	
White Blood Cells	NIDiasABP	
PTT	NIMAP	
Base Excess	NISysABP	
Calculated Total CO2	PaCO2	
Lactate	PaO2	
pCO2	pH	
pH	Platelets	
pO2	RespRate	
PT	SaO2	
Alanine Aminotransferase	SysABP	
Albumin	Temp	
Specific Gravity	TroponinI	
Potassium Chloride	TroponinT	
Calcium Gluconate	Urine	
Insulin - Regular		
Heparin Sodium		
K Phos		
Sterile Water		
Gastric Meds		
GT Flush		
LR		
Furosemide (Lasix)		
Solution		
Hydralazine		
Midazolam (Versed)		
Lorazepam (Ativan)		
PO Intake		
Insulin - Humalog		
OR Crystalloid Intake		
Morphine Sulfate		
D5 1/2NS		
Insulin - Glargin		
Metoprolol		
OR Cell Saver Intake		
Dextrose 5%		
Norepinephrine		
Packed Red Blood Cells		
Phenylephrine		
Albumin 5%		
Nitroglycerin		
KCL (Bolus)		
Magnesium Sulfate (Bolus)		
Stool Out Stool		
Urine Out Incontinent		
Ultrafiltrate Ultrafiltrate		
Gastric Gastric Tube		
Foley		
Void		
TF Residual		
Pre-Admission		
Chest Tube 1		
OR EBL		
Chest Tube 2		
Fecal Bag		
Jackson Pratt 1		
Condom Cath		
D5W		
Docuse Sodiu		
Magnesium Sulfate		
Potassium Chloride		
Bisacodyl		
Humulin-R Insulin		
Aspirin		
Sodium Chloride 0.9% Flush		
Metoprolol Tartrate		